Molecular structure-(thermo)electric property relationships in single-molecule junctions and comparisons with single and multi-parameter models

Masnun Naher,[a#] David C. Milan,[b#] Oday A. Al-Owaedi,[c#] Inco J. Planje,[b] Sören Bock,[a] Juan Hurtado-Gallego,[d] Pablo Bastante,[d] Zahra Murtada Abd Dawood,[c] Laura Rincón-García,[d] Gabino Rubio-Bollinger,[d,e] Simon J. Higgins,[b] Nicolás Agraït,[d,e,f]* Colin J. Lambert,[g]* Richard J. Nichols,[b]* Paul J. Low.[a]*

[a] School of Molecular Sciences, University of Western Australia, 35 Stirling Highway, Crawley, WA, 6009, Australia.

[b] Department of Chemistry, University of Liverpool, Crown St, Liverpool, L69 7ZD, UK.

[c] Department of Laser Physics, Women Faculty of Science, The University of Babylon, Hilla 51001, Iraq.

[d] Departamento de Física de la Materia Condensada, Universidad Autónoma de Madrid, Madrid, E-28049, Spain.

[e] Condensed Matter Physics Center (IFIMAC) and Instituto Universitario de Ciencia de Materiales "Nicolás Cabrera" (INC), Universidad Autónoma de Madrid, E-28049 Madrid, Spain.

[f] Instituto Madrileño de Estudios Avanzados en Nanociencia IMDEA-Nanociencia, E-28049 Madrid, Spain.

[g] Department of Physics, University of Lancaster, Lancaster, LA1 4YB, UK.

# These authors contributed equally

nicolas.agrait@uam.es
c.lambert@lancaster.ac.uk
R.J.Nichols@liverpool.ac.uk
paul.low@uwa.edu.au

Abstract

The most probable single-molecule conductance of each member of a series of twelve conjugated molecular wires, six of which contain either a ruthenium or platinum center centrally placed within the backbone, has been determined. The measurement of a small, positive Seebeck coefficient has established that transmission through these molecules takes place by tunneling through the tail of the HOMO resonance near the middle of the HOMO-LUMO gap in each case. Despite the general similarities in the molecular lengths and frontier-orbital compositions, experimental and computationally determined trends in molecular conductance values across this series cannot be satisfactorily explained in terms of commonly discussed 'single parameter' models of junction conductance. Rather, the trends in molecular

conductance are better rationalized from consideration of the complete molecular junction, with conductance values well described by transport calculations carried out at the DFT level of theory, based on the Landauer-Büttiker model.

Introduction

The field of molecular electronics has advanced rapidly following the development of convenient laboratory methods for the construction of electrode|molecule|electrode junctions, and measurement of their through-molecule conductance.[1-6] These molecular junctions have allowed exploration of the electrical properties of a wide range of molecular structures, establishing a number of structure-property relationships[7-9] and elementary circuit laws.[10-14] These concepts have in turn improved the design of molecular 'components' with high electrical conductance,[15-16] outstanding rectification ratios,[17] and transistor-like gated conductance.[18-22] In addition, uniquely molecular phenomena that influence the transmission of charge such as quantum interference have been identified, which provide new avenues for molecular design,[8, 23-25] and lead to proposals for molecular materials with useful properties such as an enhanced thermoelectric figure of merit, ZT, and promisingly high power factors, GS^2, where G is the conductance and S, the thermopower.[26-30] Such concepts and associated investigations contribute to a growing awareness of the potential for molecular junctions to offer desirable function.[31]

Here we report the experimental determination of the Seebeck coefficient and molecular conductance characteristics of a series of acyclic and cyclic thioether-anchored organic compounds and organometallic complexes. The Seebeck measurements establish HOMO-mediated electron transport near the middle of the

HOMO-LUMO gap, consistent with the results from DFT and non-equilibrium Green's function calculations. Despite the gross chemical similarity of these compounds, all of which display linearly π-conjugated molecular backbones and thioether-based anchor groups, the relatively poor fitting of molecular conductance values to models based on any one of a variety of single experimental parameters, including molecular length, HOMO energy, redox potential or HOMO-LUMO gap, demonstrates the need to consider a holistic model to predict and explain the electrical and thermoelectrical response of these molecular junctions.

Results and Discussion

The Molecular Wires

A group of twelve 'wire-like' molecules that exemplify a range of common molecular backbones (alkynes (**1**), 1,3-diynes (**2**), 1,4-bis(phenyl ethynyl) benzenes (**3**) and *trans*-bis(acetylide) complexes of ruthenium (**4**, **5**) and platinum (**6**)) and bear one of two different thioether contacting groups (thioanisole (**a**) and 3,3-dimethyl-2,3-dihydrobenzo[*b*]thiophene (DMBT, **b**)) were chosen for study here (Chart 1).[32] Conjugated polyyne[33-37] and 1,4-phenylene ethynylene motifs[38-39] are commonly found in many organic wire-like compounds, and the *trans*-bis(acetylide) ruthenium[40-49] and platinum[44-45, 50-52] scaffolds have been well represented in the more limited range of studies of organometallic complexes in molecular junctions reported to date. The compounds **1a**,**b** – **6a**,**b** (Chart 1) therefore provide a representative cross-section of common molecular backbones with which to explore structure-property relationships in molecular junctions, and in particular the impact of introducing a transition metal center into the molecular backbone.

The acyclic thiomethyl (SMe) anchor group is known to provide a good electrical contact to gold electrodes and is able to support either HOMO- or LUMO-based through-molecule charge transport.[53] Although less commonly employed as an anchor group, the cyclic thioether anchor group benzodihydro[*b*]thiophene (BT) has been shown to give excellent junction formation probabilities within molecular junctions. Examples of organic compounds[34, 54-55] and metal complexes[56] featuring such contacts explored to date have shown promising electrical and thermoelectrical behavior.[11, 29] Here the closely related 3,3-dimethyl-2,3-dihydrobenzo[*b*]thiophene (DMBT) derivative has been employed as an anchor group,[57] with the dimethyl groups serving to improve solubility without compromising the excellent physical characteristics of the BT-style anchor in the junction.

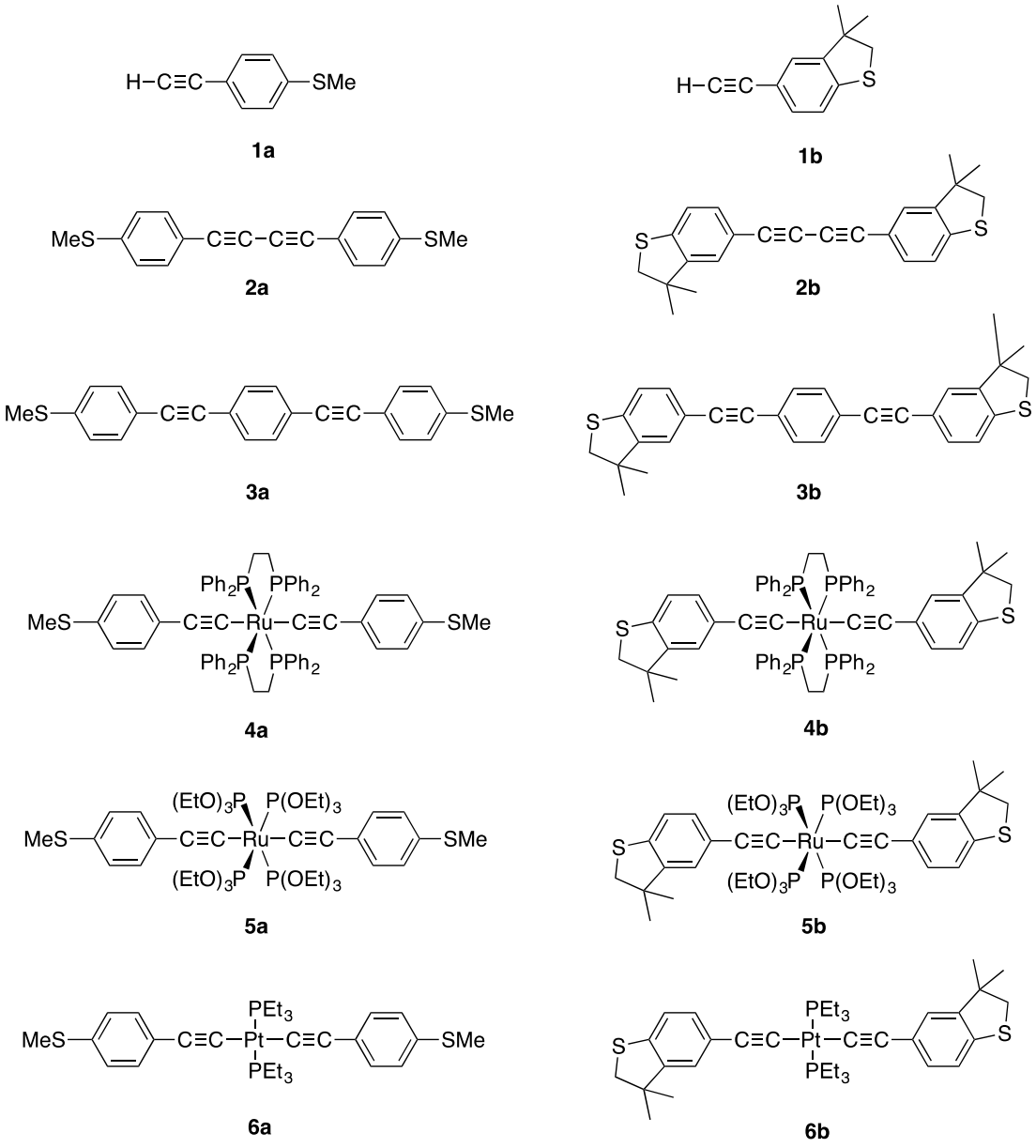

Chart 1. The compounds **1a**,**b** – **6a**,**b** used in this work.

Single Molecule Conductance and Thermopower (Seebeck coefficient) Measurements

The single molecule conductance values of compounds **1a**,**b** – **6a**,**b** were determined using data obtained from scanning tunneling microscope break junction (STM-BJ) measurements carried out in 1 mM mesitylene (containing a small fraction of THF in the case of the least soluble compounds) solution (Table 1). In each case, the

conductance histograms were constructed from ca. 3000 current-distance traces that exhibited the characteristic plateaus associated with formation of a molecular junction (Figure 1). The peaks in the conductance histograms that correspond to the most probable molecular conductance given in Table 1 were determined by fitting to a Gaussian curve in each case. The break-off distance for each molecule in the series determined from 2D plots corrected for the snap-back of the STM tip at the point of junction rupture is also listed in Table 1.[58]

Whilst terminal ethynyl moieties have been used to directly anchor molecules to gold nanoparticles[59-62] and gold[37, 63 64-66] or silver[67] electrodes within molecular junctions, to the best of our knowledge the study of **1a** and **1b** represent the first measurements of the single-molecule conductance of such simple terminal arylacetylenes. The parent acetylenes **1a** and **1b** give rise to relatively high molecular conductance values, of the order of 10^{-2} G_0 (Table 1), although the asymmetric Au-S and Au-C≡C contacts formed within the junction prohibit direct comparisons with other compounds in the series explored here.

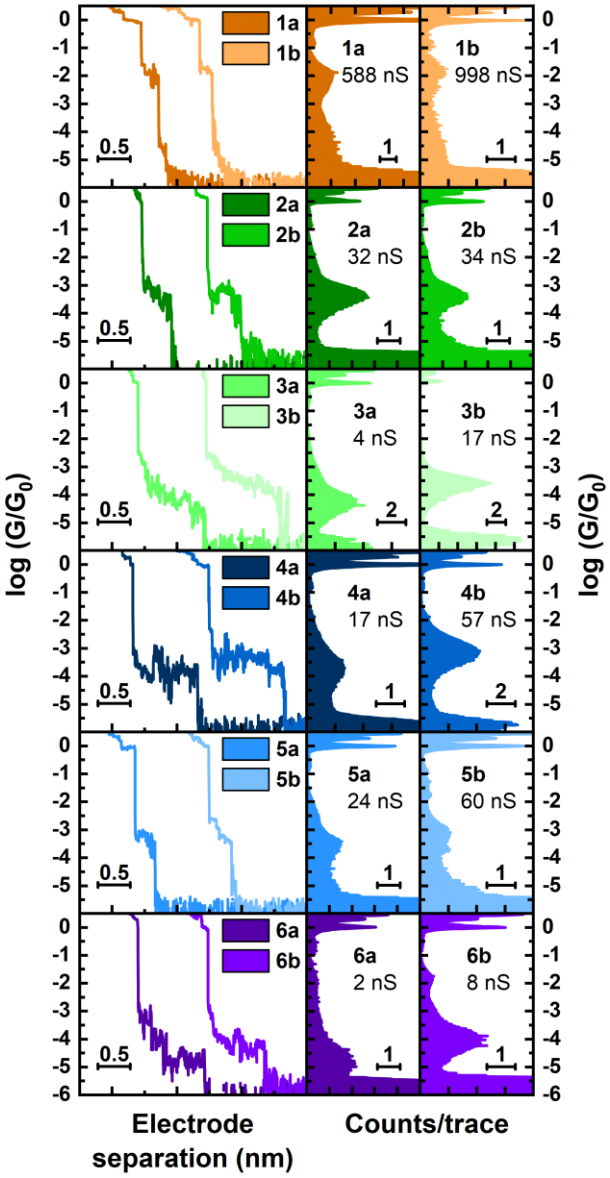

Figure 1. Representative conductance *G vs.* electrode displacement traces and conductance histograms for compounds and complexes **1a**,**b** – **6a**,**b**.

Table 1. Summary of selected experimental and computational data for **1a**,**b** – **6a**,**b**.

	$d_{S...S}$ / Å[a]	$d_{S...S}$ / Å[b]	d / Å[c]	$\log(G_{exp}/G_0)$[d]	G_{exp}/G_0[d]	$\log(G_{th}/G_0)$[e]	G_{th}/G_0[e]	Q_S[f]	ΔQ / e[g]
1a	7.17[h]	7.27[h]	6.3 ± 2.2	–2.12	76×10^{-4}	–1.51	310×10^{-4}	0.22	0.211
2a	15.71	15.84	7.6 ± 3.1	–3.39	4.1×10^{-4}	–3.44	3.6×10^{-4}	0.23	0.316
3a	20.07	20.16	10.2 ± 6.9	–4.25	0.56×10^{-4}	–4.28	0.52×10^{-4}	0.23	0.182
4a	18.58	18.71	9.3 ± 7.4	–3.65	2.2×10^{-4}	–3.73	1.9×10^{-4}	0.09	0.617
5a	18.57	18.64	7.7 ± 3.9	–3.51	3.1×10^{-4}	–3.88	1.3×10^{-4}	0.09	0.426
6a	18.47	18.71	10.7 ± 6.6	–4.66	0.22×10^{-4}	–4.72	0.19×10^{-4}	0.10	0.220
1b	7.16[h]	7.21[h]	6.3 ± 1.9	–1.89	130×10^{-4}	–1.42	380×10^{-4}	0.22	0.246
2b	15.66	15.65	8.0 ± 3.8	–3.36	4.4×10^{-4}	–3.43	3.7×10^{-4}	0.23	0.318
3b	19.99	19.91	11.0 ± 7.7	–3.66	2.2×10^{-4}	–3.88	1.3×10^{-4}	0.22	0.346
4b	18.53	18.47	11.7 ± 9.1	–3.13	7.4×10^{-4}	–3.47	3.4×10^{-4}	0.07	0.646
5b	18.30	18.23	7.5 ± 3.0	–3.11	7.8×10^{-4}	–3.23	5.9×10^{-4}	0.07	0.471
6b	18.39	18.52	9.6 ± 5.3	–3.99	1.0×10^{-4}	–4.15	0.71×10^{-4}	0.08	0.492

[a] crystallographically determined S...S distance.[32] [b] Computationally determined S…S distance from optimized (BLYP35/COSMO(CH_2Cl_2)/6-31G** (Ru, Pt LANL2DZ)) molecular geometries.[32] [c] break off distance allowing for snap-back (± 2σ).[58] [d] most probable experimentally

determined single-molecule conductance. [e] calculated single-molecule conductance. [f] charge transferred from the sulfur atoms to the electrodes in the junction. [g] charge transferred from the molecule to the electrodes in the junction. [h] (H)-*C*≡…*S* distance

An examination of the most probable single-molecule conductance values in Table 1 reveals that for each pair of compounds and complexes, the DMBT-contacted version (**b**) gives rise to modestly higher values than the SMe-contacted structural analogue (**a**). The most probable conductance values of the thio-ether contacted buta-1,3-diynes **2a** and **2b** fall near 4×10^{-4} G_0, consistent with the values reported for buta-1,3-diynes with pyridinyl, thiolate or dihydrobenzo[*b*]thiophene contacting groups.[33] The conceptual insertion of the 1,4-phenylene ring into the diyne backbone gives the oligophenylene ethynylene (OPE) style complexes **3a** and **3b**. Compared to the compounds **2** the molecular conductance of these OPE derivatives decreases by a factor of 2 (**2b** to **3b**) – 10 (**2a** to **3a**) (Table 1), but again falling in the range expected of such compounds.[68-69] Empirically, these trends can be attributed to a convolution the competing factors that influence through molecule charge transport, including the increased molecular length and changes in molecular level (orbital) alignment with the electrode Fermi level (i.e. the tunnel barrier width and height).

The insertion of metal centers within the π-conjugated backbone of an organic 'molecule wire' to modulate the tunnel barrier width and height has also attracted attention,[47-48, 70-73] and the ruthenium complexes **4a**,**b** and **5a**,**b** offer conductance values comparable to those of the shorter buta-1,3-diynes **2a**,**b**. There is little difference in the conductance of the [Ru(dppe)$_2$] based compounds (**4**) relative to the [Ru{P(OEt)$_3$}$_4$] analogues (**5**), indicating that the ancillary ligands have a relatively minor influence on molecular conductance in these compounds; the role that the alkyl phosphite ligands might play in insulating the molecular structure from the adventitious contacts of the tip to the metal-ligand moiety more prevalent with aryl-functionalized ancillary ligands has been described elsewhere.[52] Although presenting

molecular lengths comparable to the ruthenium complexes **4** and **5**, the platinum complexes **6a** and **6b** are the least conductive (most resistive) members of the set under investigation here, with most probable conductance values approximately half that of the longer OPE analogues **3a** and **3b**. The lower conductance of the thioether-anchored platinum complexes **6a** and **6b** relative to the ruthenium compounds **4a**,**b** and **5a**,**b** contrasts with the remarkably similar mid-gap conductance of comparable ruthenium and platinum bis(acetylide) complexes that are more weakly coupled within molecular junctions by 3-thienyl anchor groups.[44] A first interpretation of these data might presume a lower-lying HOMO and hence greater tunnel barrier in the case of the Pt complexes **6** as an explanation for these trends in relative conductance. However, the first (irreversible) oxidation potentials of **6a** and **6b** are somewhat more thermodynamically favorable than those of **3a** and **3b**, and estimates from either the electrochemical data or DFT calculations place the HOMO levels of the platinum complexes higher than those of the OPE systems (Table S1).[32] The higher lying HOMO is offset by a larger HOMO-LUMO gap, and that may lead to lower mid-gap conductance (Table S1).[32]

To obtain a deeper body of experimental data concerning the mechanism of molecular conductance, measurements of the thermopower (Seebeck coefficient, Figure 2) using the representative compounds and complexes **2b**, **3b**, **5b** and **6b** were made to establish the nature of the charge carriers in these thioether-contacted molecular junctions (Table 2, Figure 3).[74 75] These compounds were selected to sample the four key molecular backbones (diyne, 1,4-phenylene and *trans*-bis(acetylide) fragments of ruthenium and platinum) and where the most significant differences between their thermoelectric response might be expected. For the four selected compounds, the

thermovoltage, $\Delta V_{th,}$ that develops for temperature differences applied between the electrodes, ΔT, was measured from over 200 individual junctions, for values of ΔT between 0 and 39 K. These experiments were performed in ambient conditions and at room temperature, and G and ΔV_{th} values were simultaneously obtained by measuring small *IV* ramps (± 20 mV) while the molecular junctions were formed; further details are provided in the Supporting Information. For each ΔT-measurement, a Gaussian distribution function was fitted to each set of ΔV_{th} data (Figure S3) to give the mean value, $\overline{\Delta V_{th}}$, and the standard deviation, σ_{th}, represented by the empty circles and error bars, respectively, in the plots shown in Figure 3. In the case of compound **5b**, the data shown in Figure 3c is obtained by performing several experimental runs for each ΔT, giving as many pairs of $\overline{\Delta V_{th}}$ and σ_{th} values when the runs are considered separately. These values from individual runs are plotted as independent data sets in Figure S4 to demonstrate the robustness of the measurements.

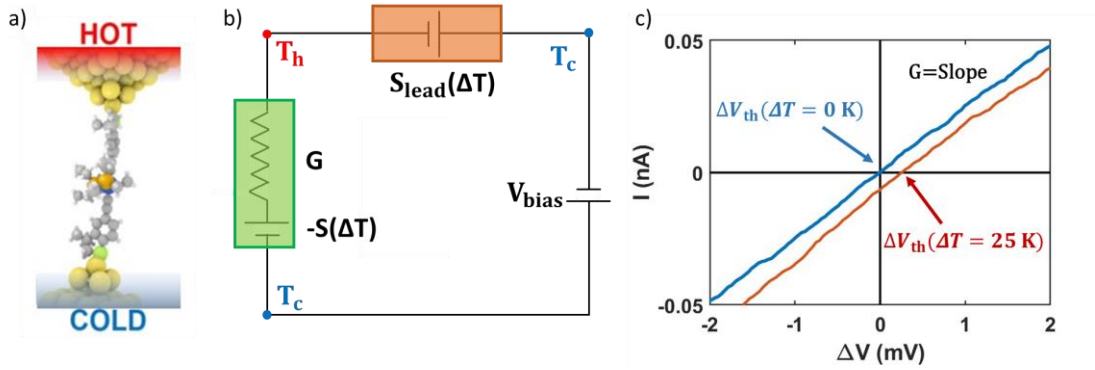

Figure 2. Thermopower experimental technique. (a) Illustration of a molecule (compound **6b**) connected between the hot tip (at temperature T_h) and the cold substrate (at temperature $T_c < T_h$). (b) Equivalent thermal-electric circuit of the STM with a temperature difference between the tip, $T_h > T_{ambient}$, and the sample, $T_c = T_{ambient}$, $\Delta T = T_h - T_c$. In this model, V_{bias} is the voltage applied to the sample, G is the

conductance of the molecular junction, and S and S_{Cu} are the Seebeck coefficient of the molecular junction and of the copper wire used to connect the heated tip ($S_{\mathrm{Cu}} = 1.85\ \mu\mathrm{V/K}$),[74] respectively. (c) Example of two *IV* curves recorded during formation of a molecular junction at $\Delta T = 0$ K (blue) and $\Delta T = 25$ K (red) (for **6b**). The thermovoltage, ΔV_{th}, and conductance, G, are the zero-current crossing point and the slope of the curve, respectively (Figure S2). The plotted *IV* data are each the mean curve between two *IV* curves recorded at the same point in the molecular junction, one from +20 to -20 mV and another one from -20 to +20 mV (Figure S1).

Table 2. Summary of the Seebeck coefficient and power factor from experimental measurements and computational modelling, for **2b**, **3b**, **5b** and **6b**.

	S / μV/K	S_{th} / μV/K	$P = GS^2$ / 10^{-18} W/K^2	$P_{th} = G_{th}S_{th}^2$ / 10^{-18} W/K^2
2b	3.7	3.7	0.43	0.87
3b	4.5	4.5	0.38	0.74
5b	7.1	6.9	2.22	1.96
6b	6.1	6.4	0.32	0.20

The Seebeck coefficient, *S*, is given by Equation 1

$$S = \frac{\Delta V_{th}}{\Delta T} \qquad (1)$$

and can therefore be obtained from the slope of a plot of all the individual experimental values ΔV_{th} versus ΔT (see linear fits in Figure 3). Note that the ΔV_{th} values measured in our experimental setup are defined $V_c - V_h$, as can be seen in the

equivalent thermal-electric circuit (Figure 2b). The values obtained range from $S = 3.7$ μV/K for compound **2b** to $S = 7.1$ μV/K for compound **5b**, with a relative error smaller than 2% for all the molecules. The positive sign of the Seebeck coefficient in all cases confirms an important role played by occupied molecular orbitals in the conductance of these compounds. However, the relatively small values of this parameter suggest that conductance takes place in the vicinity of the middle of the HOMO-LUMO gap, well removed from the steep changes in conductance versus electron energy that accompany transmission near a resonance. An important consequence of this mid-gap conductance mechanism is that only small variations in the relative position of the Fermi level would be necessary to change the sign of the Seebeck coefficient.[76]

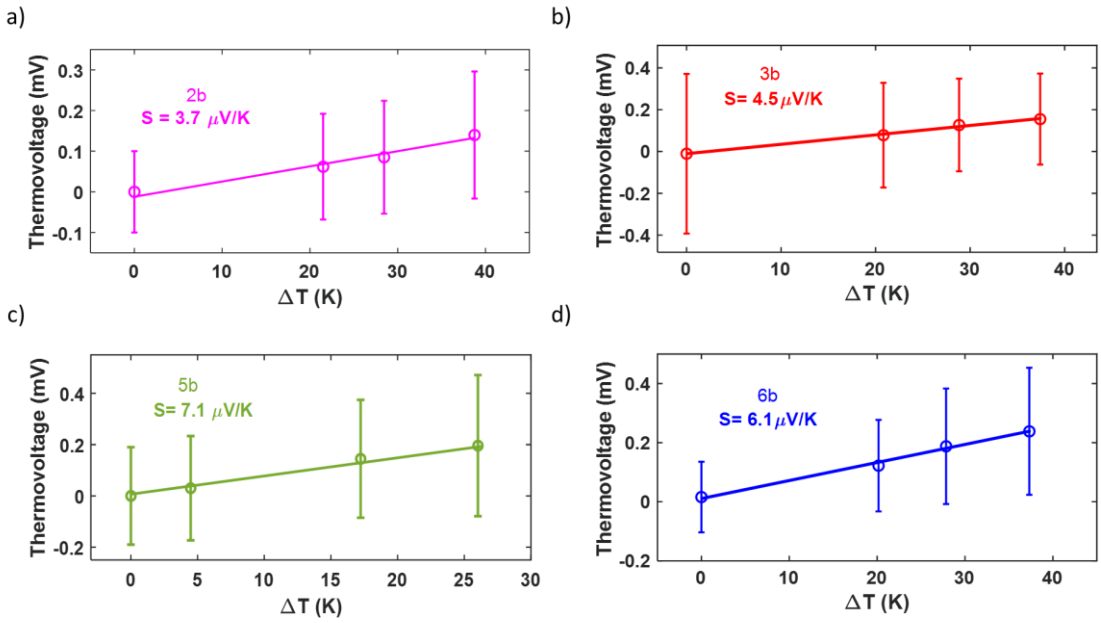

Figure 3. Thermopower results. (a-d) Thermovoltage measurements of molecules **2b**, **3b**, **5b** and **6b** for each temperature difference ΔT between the tip and the sample, from 0 to 39 K. The Seebeck values are given by the slope of the linear fit of all the individual ΔV_{th} points (numerical values are shown in

each plot). The empty circles and vertical error bars correspond to the thermovoltage mean value, $\overline{\Delta V_{\mathrm{th}}}$, and the standard deviation, σ_{th}, respectively, derived from a Gaussian fit to each set of measurements (see 1D histograms in Figure S3*)*.

From the most probable single-molecule conductance values, *G*, and the Seebeck coefficients, *S*, the power factor, *P*, which represents the capacity of a material to extract energy from the thermal difference, can also be determined (Equation 2, Table 2).

$$P = GS^2 \qquad (2)$$

Thus, whilst the Seebeck coefficients of both the metal complexes **5b** and **6b** are substantially higher than the organic compounds **2b** and **3b**, the lower conductance of the platinum compounds results in a lower overall power factor. Whilst far from optimal, the increase in the power factor *P* following introduction of the ruthenium fragment in **5b** indicates a line for further investigation with a view to the development of thermoelectric materials.

Computational Models of Molecular Junctions

The overall conductance of a molecular junction, *G*, can be described within the framework of the Landauer-Büttiker formalism (Equation 3)

$$G = \left(\frac{2e^2}{h}\right) \int_{-\infty}^{\infty} dE\, T(E)(-df\,(E)/dE) \approx \left(\frac{2e^2}{h}\right) T(E_F) \qquad (3)$$

where $T(E)$ is the transmission coefficient describing electrons of energy E passing from the left to the right electrode via the molecular backbone.[77,30-33] In this equation, $f(E)$ is the Fermi function, E_F is the Fermi energy of the electrodes. The approximation given in Equation 3 is valid provided the transmission function is approximately constant on the scale of k_BT, where T is the temperature and k_B is Boltzmann's constant. To gain an overarching view of the trends in molecular conductance, the individual junctions **1a**,**b** – **6a**,**b** were modelled as a function of the Fermi energy. In each case, the Fermi level (E_F – E_F^{DFT}) lies within the HOMO-LUMO gap, and towards the tail of the HOMO resonance (Figure 4), entirely consistent with the experimentally determined positive sign of the Seebeck coefficients.

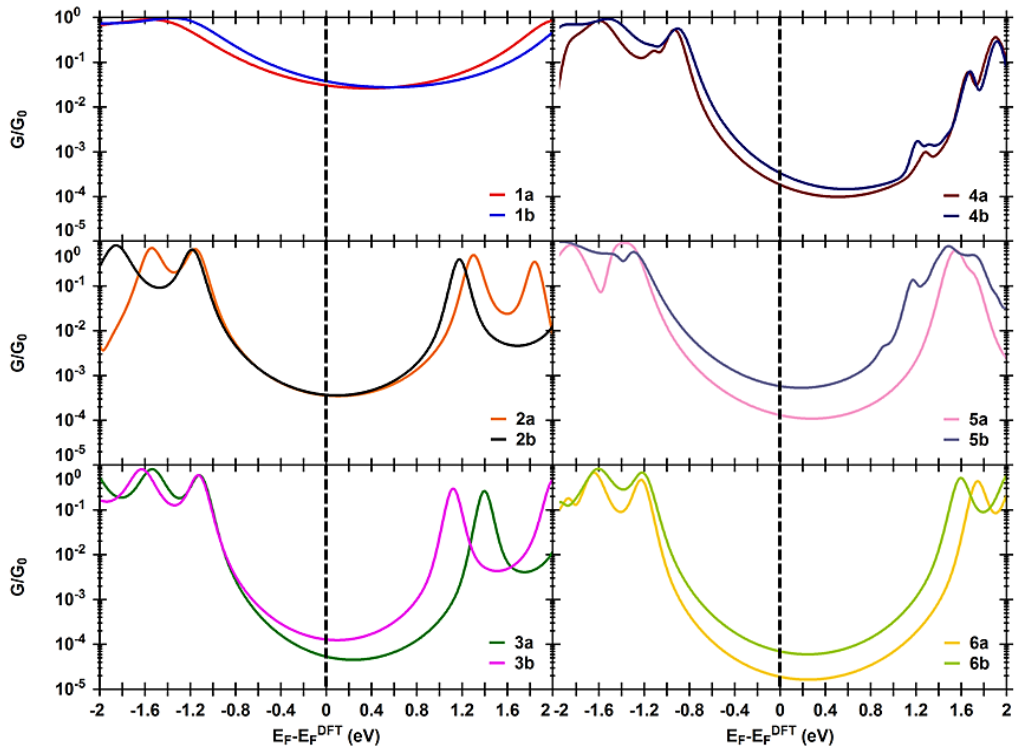

Figure 4. The calculated conductance of molecular junctions formed from compounds **1a**,**b** - **6a**,**b**. The black dashed lines show the Fermi energy in each case.

The experimentally determined and theoretical conductance data from **1a**,**b** – **6a**,**b** summarised in Table 1 may be compared in a scatter plot (Figure 5), from which it is clear that the conductance values calculated near the DFT-estimated Fermi level are in excellent agreement with the experimentally determined values over the whole series of twelve molecular wires. As discussed, for example, by Thygesen and colleagues, the energetic location of frontier molecular orbitals is determined by partial charge transfer to or from the electrodes.[78] Here the calculated charge transfer from the molecule to the electrodes ranges from ca. 0.2 – 0.6 electron, consistent with a degree of charge pinning in these junctions (ΔQ, Table 1); for each pair of compounds, the sulfur atoms of the anchor group donate a similar fraction of the total charge (Q_S, Table 1).

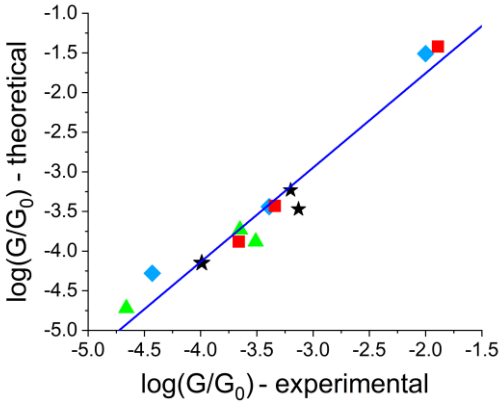

Figure 5. Scatter graph showing the correlation between the experimental measured conductance (x-axis) and the theoretical computed values (y-scale) both expressed as log(G/G_0). Data taken from Table 1, with the line provided as a guide for the eye. Blue diamonds are compounds **1a**, **2a** and **3a**; red squares are **1b**, **2b** and **3b**; green triangle are **4a**, **5a** and **6a**; black stars are **4b**, **5b** and **6b**.

Thermoelectric properties

A comparison of the experimentally determined thermoelectric properties of the molecules with the calculated values of the Seebeck coefficients and power factors is also informative. Provided the transmission function, $T(E)$, can be approximated by a straight line on the scale of k_BT, the Seebeck coefficient is given by Equation 4

$$S \approx -L|e|T\left(\frac{d\ lnT(E)}{dE}\right)_{E=E_F} \qquad (4)$$

where L is the Lorenz number $L = \left(\frac{k_B}{e}\right)^2 \frac{\pi^2}{3}$ = 2.44.10^{-8} WΩK^{-2}. In other words, S is proportional to the negative of the slope of $\ln T(E)$, evaluated at the Fermi energy (Figure S9). As noted above, the DFT calculation places the Fermi energy near the middle of the HOMO-LUMO gap, but slightly closer to the HOMO, consistent with the measured positive sign and small value of the Seebeck coefficient. The calculated thermopower (S_{th}) of compounds **2b**, **3b**, **5b** and **6b** were found to be in excellent agreement with the experimental values (Table 2).[79] From the most probable Seebeck coefficient, the power factor ($P_{th} = G_{th}S_{th}^2T$, where T = 300 K) was also calculated for each junction studied; given the agreement between experimental and theoretically predicted values of G and S over the range of compounds examined, P_{th} is also in good agreement with power factor, P, obtained from experimental data (Table 2).

Empirical Models

Empirical comparisons of the electrical properties of organic molecules with those of coordination complexes and organometallic compounds are often complicated by

differences in molecular length, and uncertainty over nature of the charge carriers (i.e. hole vs electron mediated transport) and hence molecular level(s) most critical to the transmission properties of the junction.[44, 48, 52] In contrast, the DFT calculations described in the foregoing sections, which are based on the Landauer-Büttiker description of the junction (Equation 3), gave an excellent description of the electrical and thermoelectric properties of the molecular junctions, combining the physical and chemical parameters associated with the junctions into the transmission function $T(E)$ to give a holistic description of the junction. However, the growing interest in the design of metal complexes for molecular electronics,[70-71, 73, 80] together with the desire to better inform molecular design concepts,[81-85] prompted consideration of the data presented in Table 2 against a number of the common structure-property relationships that have been developed from a range of simple models of charge transfer through a molecular junction. These comparisons are carried out with a view to better understand the appropriateness, or not, of some of the more widely employed junction models to structurally varied compound families such as **1** – **6** and provide insight to any dominant parameter operating across this range of compound backbones and anchor groups.

Correlations of Conductance with Molecular Length

In the case of the compounds studied here, the molecular lengths of < ca. 2 nm are consistent with a dominant contribution from coherent tunnelling mechanisms.[34, 42, 69] However, this molecular length alone is not a definitive measure of tunnelling and prompts greater consideration of the evidence for the transport mechanism from further experimental data and computational models.

For a simple single-channel, rectangular tunnel barrier model, conductance (G) through the barrier (the molecule) decreases exponentially with the length of the barrier (l) (Equation 5)

$$G \propto e^{-\beta l} \qquad (5)$$

This relationship has formed the basis of many explanations of conductance within families of similarly structured molecules, with the decay parameter, β, often serving as a proxy measure for the efficacy of wire-like behaviour. Plots of ln(G) vs l have also been used to infer details of the charge transport mechanism, including identification of σ-interference effects.[86] More commonly, changes in slope of the ln(G) vs. l plots leading to a shallower decay in G as a function of molecular length for longer molecules is taken as an indication of a change in the dominant transport mechanism from tunnelling to thermally activated hopping.[68, 87-88] Conductance as a function of temperature is also often considered as an indication of a dominant contribution from thermally activated hopping; however, thermal dependence is also possible within phase coherent tunnelling models due to thermal broadening of Fermi functions, and temperature-dependent conductance arising from the temperature dependence of the Fermi distribution in the leads rather than activated hopping of charge carriers has been demonstrated.[89-90]

The structures of **1a,b** – **6a**,**b** have all been determined crystallographically, with confinement of the sulfur atom within the 5-membered ring of the DMBT moiety leading to a small decrease in the S…S distance relative to the respective thioanisole analogue (Table 1). This decrease in S…S bond length is less than 0.5% for all pairs

of compounds, with the exception of **5a**,**b** for which the decrease amounts to ca. 1.5%. The same trends are apparent in the DFT optimised geometries (BLYP35/Ru, Pt LANL2DZ, all other atoms 6-31G**, COSMO CH_2Cl_2), with differences in S…S distance of the order of 1.2% for all compound pairs except **5a**,**b** where the contraction in molecular length increases to 2.2% (Table 1). These molecular parameters match with the experimentally determined break-off distances (Table 1) and the junction length of the computational models (Table 1).

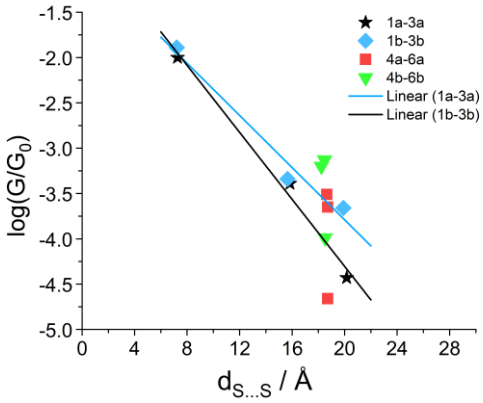

Figure 6. A plot of log(G/G_0) vs $d_{S...S}$ for compounds and complexes **1a,b** – **6a**,**b**. The linear trend lines for the organic compounds **1a** – **3a** (R^2 = 0.988) and **1b** – **3b** (R^2 = 0.972) are marked.

A plot of log(G/G_0) against the crystallographically determined $d_{S...S}$ reveals that the data from the organic compounds (**1**, **2** and **3**) follow a reasonably consistent linear trend for each binding group (SMe (**a**) apparent β = 0.43 $Å^{-1}$, DMBT (**b**) apparent β = 0.33 $Å^{-1}$), which is largely in line with expectations of the increasing length and insertion of the central 1,4-phenylene moiety in **3** (Figure 6). However, in the case of the metal complexes **4**, **5** and **6** conductance variations of up to one order of magnitude are observed with little change in molecular length (Table 1, Figure 6).

Therefore, whilst the molecular junctions formed with the organic compounds seem to be well described as a series of closely related tunnel barriers, the metal complexes present additional complexity that is not accurately captured in a simple distance dependence model. However, these complexities are captured by the DFT modelling of junction conductance (Figure 5). This highlights the notable changes in electronic structure between the metal complexes **4** - **6**, while their length remains comparable.

Correlation of conductance with molecular orbital energies

A more complete description of the molecular junction in terms of off-resonant transport through a rectangular barrier not only includes the tunnel barrier length, *l*, but also the barrier height (Equation 6). Given the positive Seebeck coefficient, and hence implications of HOMO-mediated transport, the barrier height can initially be approximated as the energy difference of the Au-electrode Fermi level and the molecular HOMO.[91]

$$G \propto e^{-\Delta E l} \qquad (6)$$

Molecular HOMO energy levels are often estimated from experimentally determined oxidation potentials relative to an internal redox marker such as ferrocene (E_{HOMO} = 4.8 eV), such that $\Delta E = \sqrt{E_{HOMO} - E_{Au}}$ or DFT calculations, and compared with the work function of a clean, bare gold(111) surface (E_{Au} = –5.3 eV).[91] In the case of the ruthenium *trans*-bis(acetylide) complexes **4** and **5** here, DFT estimates of the HOMO energy (Table S1) are similar to those of the Tanaka polyyndiyl complexes,[47] falling

near –4.30 eV; however, molecular conductance values of **4** and **5** are approximately an order of magnitude lower, despite the rather similar molecular length.

Venkataraman has used E_{Au} as a fitting parameter in Equation 6, with estimates of E_{HOMO} for a series of aromatic diamines made from electrochemical measurements.[91] Although the poor electrochemical response of the organic compounds and platinum complexes restricted the capacity to determine an accurate half-wave potential from voltammetric methods (Table S1), by using DFT calculated E_{HOMO} values instead of the data fall onto two relatively straight-line relationships vs fitted values of E_{Au} for the organic compounds **1 – 3** (E_{Au} = 4.6 eV) and organometallic complexes **4 – 6** (E_{Au} = 4.2 eV) (Figure 7). These values for E_{Au} compare well with estimates of the work function of gold covered with SAMs of organic molecules; for instance, the value of ~4.3 eV from Zangmeister et al. for a SAM of para-ethynylphenyl thiol on gold.[92] Given the inherent approximations in the DFT determined HOMO energy levels, and the additional uncertainty in these molecular levels in the junction introduced from the charge transfer and the Fermi level estimate such agreements are remarkable, and may well be a consequence of fortuitous cancellation of errors. However, the empirical result suggests that molecular conductance among the most structurally similar organic compounds and metal complexes can be described, at least to a first approximation, by the height and length of a model rectangular tunnel barrier.

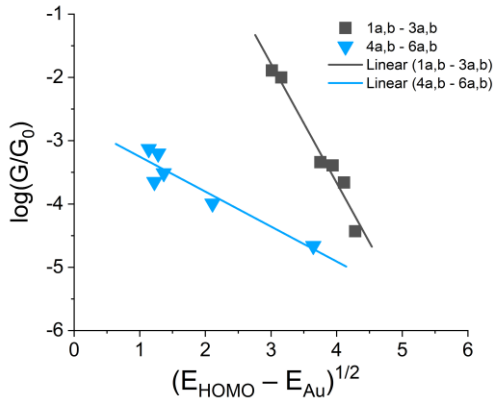

Figure 7. Plots of log (G/G_0) vs $(E_{HOMO} - E_{Au})^{1/2}$ (DFT)

The role of the anchor group

The anchor groups play a critical role in the electrical behaviour of a molecular junction,[93-96] and as such the comparisons of the compounds and complexes in the thioanisole-contacted (SMe, **a**) and 3,3-dimethyl-2,3-dihydrobenzo[*b*]thiophene (DMBT, **b**) series is informative. For each pair of complexes, the DMBT-contacted example (**b**) gives rise to a somewhat higher conductance than the SMe-contacted analogue (**a**) (Table 1, Figure 1). This can be attributed to the greater charge transferred from the DMBT-contacted compounds relative to the SMe-contacted analogues (ΔQ, Table 1). The greater charge transfer calculated for the DMBT-contacted compounds is likely correlated with the greater binding energy (BE) between the DMBT-contacted molecules and gold electrodes vs the SMe-anchored compounds, illustrated in Figure S10 for **2a** and **2b**. In the case of **2a** and **2b**, Δ(BE) = –0.09 eV, which is more than three times k_BT at room temperature, and illustrates the stronger electronic coupling between the DMBT-contacted molecules and the gold electrodes.

The conductance of symmetrically contacted molecules within a molecular junction can also be expressed in terms of the 'quantum circuit rules'.[10-11, 97-98] Assuming weak molecule-electrode electronic coupling and off-resonant tunnelling mechanisms, the conductance ratios of molecules of general form A-X-A (G_{AXA}) and B-X-B (G_{BXB}), where A and B are anchor groups and X a molecular bridge, is independent of X, i.e. in the weak coupling limit, one expects the ratio G_{AXA}/G_{BXB} to be independent of the core X. It follows that $\log(G_{AXA}) - \log(G_{BXB})$ will also be independent of the bridge, which provides a convenient basis to compare the conductance behaviour of the SMe- and DMBT-contacted compounds **2a**,**b** – **6a**,**b** (Table 3).

Table 3. A summary of quantum circuit rule $\log(G_{AXA}) - \log(G_{BXB})$ calculations for **1a**,**b – 6a**,**b**

compound type, ***N***	$\log(G_{\boldsymbol{N}\mathbf{a}}) - \log(G_{\boldsymbol{N}\mathbf{b}})$
2	0.05
3	0.77
4	0.52
5	0.31
6	0.61

The circuit rule seems to hold best for compounds based on the diethynyl benzene (**3**), *trans*-bis(ethynyl) ruthenium bis(diphenylphosphinoethane) (**4**) and *trans*-bis(ethynyl) platinum bis(triethylphosphine) (**6**) cores, since these compounds collectively possess

similar log($G_{N\mathbf{a}}$) – log($G_{N\mathbf{b}}$) values (***N*** = **3**, **4**, **6**). Clearly the greatest deviation occurs for the buta-1,3-diyne (***N*** = **2**) indicating that this bridge is more strongly coupled to the contacts than those with other moieties inserted between the triple bonds (remembering here that the quantum circuit rules are less likely to be held for more strongly coupled systems). The next greatest deviation occurs for the *pseudo*-D_{4h} *trans*-bis(ethynyl) ruthenium tetrakis(triethylphosphite) **5**, which like compound **2**, possesses a cylindrically symmetrical molecular core, which may play a role in decreasing fluctuations in the molecular π-system as a function of conformational changes around the long molecular axis, and increase the electronic coupling across the molecular junction and the electrodes.

In addition, for molecules with a given anchor group, A, and different molecular cores (A-X-A and A-Y-A), the conductance ratio G_{AXA}/G_{AYA} should be independent of the anchor A. It follows that for a series of compounds with different anchors (A, B) and backbones (X, Y) that

$$log(G_{AXA}) - log(G_{AYA}) = log(G_{BXB}) - log(G_{BYB})$$

Across the range of compounds **2a**,**b** – **6a**,**b** this quantum circuit rule generally holds true within a degree of reasonable precision given the uncertainties in the experimental data (i.e. within a factor of ca. 2 of the logarithmic values) (Table 4). For example, from the conductance data in Table 1 applying the circuit rule to **3a**,**b** and **4a**,**b** gives

$$log(G_{\mathbf{3a}}) - log(G_{\mathbf{4a}}) = -0.60$$

and

$log(G_{\mathbf{3b}}) - log(G_{\mathbf{4b}}) = -0.53$

Again, the greatest deviations from the circuit law arise from comparisons with compounds **2** and **5**.

Table 4. A summary of the numerical difference $log(G_{\mathbf{Na}}) - log(G_{\mathbf{Nb}})$ using data in Table 1. Comparison should be made of numerical values within a given set of same coloured cells, for testing the quantum circuit rule $log(G_{AXA}) - log(G_{AYA}) = log(G_{BXB}) - log(G_{BYB})$.

	2a	**2b**	**3a**	**3b**	**4a**	**4b**	**5a**	**5b**	**6a**	**6b**
2a			0.86		0.26		0.12		1.27	
2b				0.30		-0.23		-0.25		0.63
3a	-0.86				-0.60		-0.74		0.41	
3b		-0.30				-0.53		-0.55		0.33
4a	-0.26		0.60				-0.14		1.01	
4b		0.23		0.53				0.02		0.86
5a	-0.12		0.74		0.14				1.15	
5b		0.25		0.55		-0.02				0.88
6a	-1.27		-0.41		-1.01		-1.15			
6b		-0.63		-0.33		-0.86		-0.88		

Conclusions

The single-molecule conductance of a series of twelve molecular wires, six of which contain metal centers, has been measured using scanning tunneling microscopy break-junction (STM-BJ) methods. The experimentally measured values have been analyzed by DFT computations of junction conductance and this is compared to empirical models, which consider the junction lengths and frontier orbital energies against a simple tunneling barrier model. The results presented here provide confirmation of the role that the metal center can play in manipulating the conductance of a molecular junction featuring a conjugated molecule, and clarification of the underlying transport mechanisms.

The small, positive Seebeck coefficient determined experimentally has established that transmission through these molecules takes place by tunneling through the tail of the HOMO resonance near the middle of the HOMO-LUMO gap. These thermopower measurements are rare examples of the determination of the Seebeck coefficient for organometallic complexes within single-molecule junctions. The increases in both the Seebeck coefficient, *S*, and the power factor, *P*, following the introduction of a ruthenium(II)fragment within the molecular backbone provides some promising indications of the further roles that metal complexes may be yet to play in the development of molecular electronic materials.

The correlation between the DFT measured conductance values and their experimental counterparts is very good across the whole series of twelve molecular wires. In terms of empirical modeling, the linear relationships between junction

conductance, molecular length and redox potential observed for the compounds **2**, **3**, **4** and **5** can be roughly modeled within the framework of a coherent tunneling model. Whilst contributions from thermally activated conductance have not been explored, the length dependence of conductance, general adherence to quantum circuit rules and correlations of Seebeck coefficients with conductance measurements all support a dominant tunnelling mechanism.

In the case of the ruthenium compounds **4** and **5**, the metal *d*-orbitals which intimately mix with the organic π-system gives rise to a higher-lying frontier molecular orbital, which increases conductance relative to organic compounds **2** and **3** even when allowing for variations in molecular length. The platinum complexes **6** convolute the effects of tunnel barrier height and width with a larger HOMO-LUMO gap, ultimately giving molecular conductance values comparable with those of the slightly shorter OPE derivatives **3**. Together, these observations provide clarification of results and patterns of behavior in single-molecule conductance studies with metal complexes in molecular junctions and point to a clear and efficient design strategy for the further enhancement of junction conductance and Seebeck coefficients, provided Fermi energy pinning can be alleviated.

Acknowledgments

The authors thank the U.K. Engineering and Physical Sciences Research Council (EPSRC) for financial support under Grants EP/M005046/1, EP/M029522/1, EP/M014169/1 and EP/K007785/1. The Australian Research Council (ARC) is thanked for financial support under the Discovery Program (DP190100073; DP190100074). M.N. holds a Forrest Scholarship from the Forrest Research

Foundation. D.C.M. gratefully acknowledges the School of Physical Sciences Postdoctoral Development Award of the University of Liverpool for financial support. This work was further supported by the EC H2020 FET Open project grant agreement number 767187 'QuIET'. N.A. and G.R.-B. acknowledge funding from the Comunidad de Madrid NANOMAGCOST-CM (P2018/NMT-4321) and from the Spanish Ministry of Science and Innovation, through grants MAT2017-88693-R and the "María de Maeztu" Programme for Units of Excellence in R&D (CEX2018-000805-M). N.A. and L.R.-G. acknowledge funding from the Education and Research Council of the Comunidad de Madrid and the European Social Fund (Ref. PEJD-2019-POST/IND-16353). O. A. A. and Z. M. A. D. are grateful for the support from the Iraqi ministry of higher education and scientific research. The authors gratefully acknowledge the facilities, and the scientific and technical assistance of Microscopy Australian at the Centre for Microscopy, Characterisation & Analysis, The University of Western Australia, a facility funded by the University, State and Commonwealth Governments.

Author Contributions

MN and SB contributed to the molecular design strategies and synthesized the compounds and complexes. DCM led the molecular conductance studies with IJP and carried out the thermopower measurements and data analysis. JHG, PB, LRG and GRB assisted with the thermopower measurements, data collection and interpretation. OAA and ZMAD carried out the computational studies and data interpretation. SJH contributed to the molecular design concepts and data interpretations. NA led the thermopower studies and edited the manuscript with LRG and JHG. CJL led the computational work and wrote the theory sections. RJN discussed the interpretation of

the STM data and edited the manuscript. PJL conceived and led the study, coordinated the collaborations and wrote the manuscript.

Supporting Information:

Details of single-molecule and thermopower measurements.

Electrochemical data and computational HOMO energy levels.

Details of theoretical and computational studies of molecular junctions.

Geometries of model molecular junctions.

Plots of transmission functions, T(E) vs electron energy.

Plots of [–dT(E)/dE] vs Fermi energy.

Plot of the binding energy of compounds **2a** and **2b** attached to gold electrodes as a function of molecule-gold optimal distance.

In addition, single molecule data is available in the University of Liverpool data catalogue (collection #1142) at the address

https://doi.org/10.17638/datacat.liverpool.ac.uk/1142

References

1. Wang, L.; Wang, L.; Zhang, L.; Xiang, D., Advance of Mechanically Controllable Break Junction for Molecular Electronics. *Top. Cur. Chem.* **2017,** *375*, 61.
2. Vilan, A.; Aswal, D.; Cahen, D., Large-Area, Ensemble Molecular Electronics: Motivation and Challenges. *Chem. Rev.* **2017,** *117*, 4248-4286.
3. Komoto, Y.; Fujii, S.; Iwane, M.; Kiguchi, M., Single-molecule junctions for molecular electronics. *J. Mater. Chem. C* **2016,** *4*, 8842-8858.
4. Kiguchi, M.; Kaneko, S., Single molecule bridging between metal electrodes. *Phys. Chem. Chem. Phys.* **2013,** *15*, 2253-2267.
5. Nichols, R. J.; Higgins, S. J., Single-Molecule Electronics: Chemical and Analytical Perspectives. *Annu. Rev. Anal. Chem.* **2015,** *8*, 389-417.
6. Nichols, R. J.; Haiss, W.; Higgins, S. J.; Leary, E.; Martin, S.; Bethell, D., The experimental determination of the conductance of single molecules. *Phys. Chem. Chem. Phys.* **2010,** *12*, 2801-2815.

7. Su, T. A.; Neupane, M.; Steigerwald, M. L.; Venkataraman, L.; Nuckolls, C., Chemical principles of single-molecule electronics. *Nat. Rev. Mater.* **2016,** *1*, 1-15.
8. Lambert, C. J.; Liu, S. X., A Magic Ratio Rule for Beginners: A Chemist's Guide to Quantum Interference in Molecules. *Chem. Eur. J.* **2018,** *24*, 4193-4201.
9. Leary, E.; La Rosa, A.; Gonzalez, M. T.; Rubio-Bollinger, G.; Agrait, N.; Martin, N., Incorporating single molecules into electrical circuits. The role of the chemical anchoring group. *Chem. Soc. Rev.* **2015,** *44*, 920-942.
10. Manrique, D. Z.; Huang, C.; Baghernejad, M.; Zhao, X. T.; Al-Owaedi, O. A.; Sadeghi, H.; Kaliginedi, V.; Hong, W. J.; Gulcur, M.; Wandlowski, T.; Bryce, M. R.; Lambert, C. J., A quantum circuit rule for interference effects in single-molecule electrical junctions. *Nat. Commun.* **2015,** *6*, 6389.
11. Manrique, D. Z.; Al-Galiby, Q.; Hong, W. J.; Lambert, C. J., A New Approach to Materials Discovery for Electronic and Thermoelectric Properties of Single-Molecule Junctions. *Nano Lett.* **2016,** *16*, 1308-1316.
12. Liao, K. C.; Hsu, L. Y.; Bowers, C. M.; Rabitz, H.; Whitesides, G. M., Molecular Series-Tunneling Junctions. *J. Am. Chem. Soc.* **2015,** *137*, 5948-5954.
13. Vazquez, H.; Skouta, R.; Schneebeli, S.; Kamenetska, M.; Breslow, R.; Venkataraman, L.; Hybertsen, M. S., Probing the conductance superposition law in single-molecule circuits with parallel paths. *Nat. Nanotechnol.* **2012,** *7*, 663-667.
14. Seth, C.; Kaliginedi, V.; Suravarapu, S.; Reber, D.; Hong, W. J.; Wandlowski, T.; Lafolet, F.; Broekmann, P.; Royal, G.; Venkatramani, R., Conductance in a bis-terpyridine based single molecular breadboard circuit. *Chem. Sci.* **2017,** *8*, 1576-1591.
15. Carini, M.; Ruiz, M. P.; Usabiaga, I.; Fernandez, J. A.; Cocinero, E. J.; Melle-Franco, M.; Diez-Perez, I.; Mateo-Alonso, A., High conductance values in pi-folded molecular junctions. *Nat. Commun.* **2017,** *8*, 15195.
16. Wang, K.; Vezzoli, A.; Grace, I. M.; McLaughlin, M.; Nichols, R. J.; Xu, B. Q.; Lambert, C. J.; Higgins, S. J., Charge transfer complexation boosts molecular conductance through Fermi level pinning. *Chem. Sci.* **2019,** *10*, 2396-2403.
17. Chen, X. P.; Roemer, M.; Yuan, L.; Du, W.; Thompson, D.; del Barco, E.; Nijhuis, C. A., Molecular diodes with rectification ratios exceeding 10(5) driven by electrostatic interactions. *Nat. Nanotechnol.* **2017,** *12*, 797-803.
18. Song, H., Electrostatic Gate Control in Molecular Transistors. *Top. Curr. Chem.* **2018,** *376*, 37.
19. Richter, S.; Mentovich, E.; Elnathan, R., Realization of Molecular-Based Transistors. *Adv. Mater.* **2018,** *30*, 1706941.
20. Guo, S. Y.; Artes, J. M.; Diez-Perez, I., Electrochemically-gated single-molecule electrical devices. *Electrochim. Acta* **2013,** *110*, 741-753.
21. Kay, N. J.; Higgins, S. J.; Jeppesen, J. O.; Leary, E.; Lycoops, J.; Ulstrup, J.; Nichols, R. J., Single-Molecule Electrochemical Gating in Ionic Liquids. *J. Am. Chem. Soc.* **2012,** *134*, 16817-16826.
22. Osorio, H. M.; Catarelli, S.; Cea, P.; Gluyas, J. B. G.; Hartl, F.; Higgins, S. J.; Leary, E.; Low, P. J.; Martin, S.; Nichols, R. J.; Tory, J.; Ulstrup, J.; Vezzoli, A.; Milan, D. C.; Zeng, Q., Electrochemical Single-Molecule Transistors with Optimized Gate Coupling. *J. Am. Chem. Soc.* **2015,** *137*, 14319-14328.

23. Lambert, C. J., Basic concepts of quantum interference and electron transport in single-molecule electronics. *Chem. Soc. Rev.* **2015,** *44*, 875-888.
24. Solomon, G. C.; Bergfield, J. P.; Stafford, C. A.; Ratner, M. A., When "small" terms matter: Coupled interference features in the transport properties of cross-conjugated molecules. *Beilstein J. Nanotech.* **2011,** *2*, 862-871.
25. Andrews, D. Q.; Solomon, G. C.; Van Duyne, R. P.; Ratner, M. A., Single Molecule Electronics: Increasing Dynamic Range and Switching Speed Using Cross-Conjugated Species. *J. Am. Chem. Soc.* **2008,** *130*, 17309-17319.
26. Famili, M.; Grace, I. M.; Al-Galiby, Q.; Sadeghi, H.; Lambert, C. J., Toward High Thermoelectric Performance of Thiophene and Ethylenedioxythiophene (EDOT) Molecular Wires. *Adv. Funct. Mater.* **2018,** *28*, 1703135.
27. Al-Galiby, Q. H.; Sadeghi, H.; Manrique, D. Z.; Lambert, C. J., Tuning the Seebeck coefficient of naphthalenediimide by electrochemical gating and doping. *Nanoscale* **2017,** *9*, 4819-4825.
28. Lambert, C. J.; Sadeghi, H.; Al-Galiby, Q. H., Quantum-interference-enhanced thermoelectricity in single molecules and molecular films. *C. R. Phys.* **2016,** *17*, 1084-1095.
29. Sadeghi, H.; Sangtarash, S.; Lambert, C. J., Oligoyne Molecular Junctions for Efficient Room Temperature Thermoelectric Power Generation. *Nano Lett.* **2015,** *15*, 7467-7472.
30. Garcia-Suarez, V. M.; Lambert, C. J.; Manrique, D. Z.; Wandlowski, T., Redox control of thermopower and figure of merit in phase-coherent molecular wires. *Nanotechnology* **2014,** *25*, 205402.
31. Aradhya, S. V.; Venkataraman, L., Single-molecule junctions beyond electronic transport. *Nat. Nanotechnol.* **2013,** *8*, 399-410.
32. Naher, M.; Bock, S.; Langtry, Z. M.; O'Malley, K. M.; Sobolev, A. N.; Skelton, B. E.; Korb, M.; Low, P. J., Synthesis, structure and physical properties of ‘wire-like’ metal complexes. *Organometallics* **2020**, *39*, 4667 - 4687.
33. Wang, C. S.; Batsanov, A. S.; Bryce, M. R.; Martin, S.; Nichols, R. J.; Higgins, S. J.; Garcia-Suarez, V. M.; Lambert, C. J., Oligoyne Single Molecule Wires. *J. Am. Chem. Soc.* **2009,** *131*, 15647-15654.
34. Moreno-Garcia, P.; Gulcur, M.; Manrique, D. Z.; Pope, T.; Hong, W. J.; Kaliginedi, V.; Huang, C. C.; Batsanov, A. S.; Bryce, M. R.; Lambert, C.; Wandlowski, T., Single-Molecule Conductance of Functionalized Oligoynes: Length Dependence and Junction Evolution. *J. Am. Chem. Soc.* **2013,** *135*, 12228-12240.
35. Milan, D. C.; Krempe, M.; Ismael, A. K.; Movsisyan, L. D.; Franz, M.; Grace, I.; Brooke, R. J.; Schwarzacher, W.; Higgins, S. J.; Anderson, H. L.; Lambert, C. J.; Tykwinski, R. R.; Nichols, R. J., The single-molecule electrical conductance of a rotaxane-hexayne supramolecular assembly. *Nanoscale* **2017,** *9*, 355-361.
36. Milan, D. C.; Al-Owaedi, O. A.; Oerthel, M. C.; Marques-Gonzalez, S.; Brooke, R. J.; Bryce, M. R.; Cea, P.; Ferrer, J.; Higgins, S. J.; Lambert, C. J.; Low, P. J.; Manrique, D. Z.; Martin, S.; Nichols, R. J.; Schwarzacher, W.; Garcia-Suarez, V. M., Solvent Dependence of the Single Molecule Conductance of Oligoyne-Based Molecular Wires. *J. Phys. Chem. C* **2016,** *120*, 15666-15674.
37. Moneo, A.; Gonzalez-Orive, A.; Bock, S.; Fenero, M.; Herrer, I. L.; Milan, D. C.; Lorenzoni, M.; Nichols, R. J.; Cea, P.; Perez-Murano, F.; Low, P. J.; Martin, S., Towards molecular electronic devices based on 'all-carbon' wires. *Nanoscale* **2018,** *10*, 14128-14138.

38. Frisenda, R.; Stefani, D.; van der Zant, H. S. J., Quantum Transport through a Single Conjugated Rigid Molecule, a Mechanical Break Junction Study. *Acc. Chem. Res.* **2018,** *51*, 1359-1367.
39. Kaliginedi, V.; Moreno-Garcia, P.; Valkenier, H.; Hong, W. J.; Garcia-Suarez, V. M.; Buiter, P.; Otten, J. L. H.; Hummelen, J. C.; Lambert, C. J.; Wandlowski, T., Correlations between Molecular Structure and Single-Junction Conductance: A Case Study with Oligo(phenylene-ethynylene)-Type Wires. *J. Am. Chem. Soc.* **2012,** *134*, 5262-5275.
40. Liu, K.; Wang, X. H.; Wang, F. S., Probing Charge Transport of Ruthenium-Complex-Based Molecular Wires at the Single-Molecule Level. *ACS Nano* **2008,** *2*, 2315-2323.
41. Luo, L.; Benameur, A.; Brignou, P.; Choi, S. H.; Rigaut, S.; Frisbie, C. D., Length and Temperature Dependent Conduction of Ruthenium-Containing Redox-Active Molecular Wires. *J. Phys. Chem. C* **2011,** *115*, 19955-19961.
42. Kim, B.; Beebe, J. M.; Olivier, C.; Rigaut, S.; Touchard, D.; Kushmerick, J. G.; Zhu, X. Y.; Frisbie, C. D., Temperature and length dependence of charge transport in redox-active molecular wires incorporating ruthenium(II) bis(σ-arylacetylide) complexes. *J. Phys. Chem. C* **2007,** *111*, 7521-7526.
43. Marques-Gonzalez, S.; Yufit, D. S.; Howard, J. A. K.; Martin, S.; Osorio, H. M.; Garcia-Suarez, V. M.; Nichols, R. J.; Higgins, S. J.; Cea, P.; Low, P. J., Simplifying the conductance profiles of molecular junctions: the use of the trimethylsilylethynyl moiety as a molecule-gold contact. *Dalton Trans* **2013,** *42*, 338-341.
44. Bock, S.; Al-Owaedi, O. A.; Eaves, S. G.; Milan, D. C.; Lemmer, M.; Skelton, B. W.; Osorio, H. M.; Nichols, R. J.; Higgins, S. J.; Cea, P.; Long, N. J.; Albrecht, T.; Martin, S.; Lambert, C. J.; Low, P. J., Single-Molecule Conductance Studies of Organometallic Complexes Bearing 3-Thienyl Contacting Groups. *Chem. Eur. J.* **2017,** *23*, 2133-2143.
45. Al-Owaedi, O. A.; Milan, D. C.; Oerthel, M. C.; Bock, S.; Yufit, D. S.; Howard, J. A. K.; Higgins, S. J.; Nichols, R. J.; Lambert, C. J.; Bryce, M. R.; Low, P. J., Experimental and Computational Studies of the Single-Molecule Conductance of Ru(II) and Pt(II) trans-Bis(acetylide) Complexes. *Organometallics* **2016,** *35*, 2944-2954.
46. Ezquerra, R.; Eaves, S. G.; Bock, S.; Skelton, B. W.; Perez-Murano, F.; Cea, P.; Martin, S.; Low, P. J., New routes to organometallic molecular junctions via a simple thermal processing protocol. *J. Mater. Chem. C* **2019,** *7*, 6630-6640.
47. Tanaka, Y.; Kato, Y.; Tada, T.; Fujii, S.; Kiguchi, M.; Akita, M., "Doping" of Polyyne with an Organometallic Fragment Leads to Highly Conductive Metallapolyyne Molecular Wire. *J. Am. Chem. Soc.* **2018,** *140*, 10080-10084.
48. Sugimoto, K.; Tanaka, Y.; Fujii, S.; Tada, T.; Kiguchi, M.; Akita, M., Organometallic molecular wires as versatile modules for energy-level alignment of the metal-molecule-metal junction. *Chem. Commun.* **2016,** *52*, 5796-5799.
49. Zhang, L. Y.; Duan, P.; Wang, J. Y.; Zhang, Q. C.; Chen, Z. N., Ruthenium(II) as Conductive Promoter To Alleviate Conductance Attenuation in Oligoynyl Chains. *J. Phys. Chem. C* **2019,** *123*, 5282-5288.
50. Mayor, M.; von Hanisch, C.; Weber, H. B.; Reichert, J.; Beckmann, D., A trans-platinum(II) complex as a single-molecule insulator. *Angew. Chem. Int. Ed.* **2002,** *41*, 1183-1186.

51. Schull, T. L.; Kushmerick, J. G.; Patterson, C. H.; George, C.; Moore, M. H.; Pollack, S. K.; Shashidhar, R., Ligand effects on charge transport in platinum(II) acetylides. *J. Am. Chem. Soc.* **2003,** *125*, 3202-3203.
52. Al-Owaedi, O. A.; Bock, S.; Milan, D. C.; Oerthel, M. C.; Inkpen, M. S.; Yufit, D. S.; Sobolev, A. N.; Long, N. J.; Albrecht, T.; Higgins, S. J.; Bryce, M. R.; Nichols, R. J.; Lambert, C. J.; Low, P. J., Insulated molecular wires: inhibiting orthogonal contacts in metal complex based molecular junctions. *Nanoscale* **2017,** *9*, 9902-9912.
53. Dell, E. J.; Capozzi, B.; Xia, J. L.; Venkataraman, L.; Campos, L. M., Molecular length dictates the nature of charge carriers in single-molecule junctions of oxidized oligothiophenes. *Nat. Chem.* **2015,** *7*, 209-214.
54. Liu, J. Y.; Zhao, X. T.; Al-Galiby, Q.; Huang, X. Y.; Zheng, J. T.; Li, R. H.; Huang, C. C.; Yang, Y.; Shi, J.; Manrique, D. Z.; Lambert, C. J.; Bryce, M. R.; Hong, W. J., Radical-Enhanced Charge Transport in Single-Molecule Phenothiazine Electrical Junctions. *Angew. Chem. Int. Ed.* **2017,** *56*, 13061-13065.
55. Li, Y. H.; Baghernejad, M.; Qusiy, A. G.; Manrique, D. Z.; Zhang, G. X.; Hamill, J.; Fu, Y. C.; Broekmann, P.; Hong, W. J.; Wandlowski, T.; Zhang, D. Q.; Lambert, C., Three-State Single-Molecule Naphthalenediimide Switch: Integration of a Pendant Redox Unit for Conductance Tuning. *Angew. Chem. Int. Ed.* **2015,** *54*, 13586-13589.
56. Ozawa, H.; Baghernejad, M.; Al-Owaedi, O. A.; Kaliginedi, V.; Nagashima, T.; Ferrer, J.; Wandlowski, T.; Garcia-Suarez, V. M.; Broekmann, P.; Lambert, C. J.; Haga, M., Synthesis and Single-Molecule Conductance Study of Redox-Active Ruthenium Complexes with Pyridyl and Dihydrobenzo[*b*]thiophene Anchoring Groups. *Chem. Eur. J.* **2016,** *22*, 12732-12740.
57. Meisner, J. S.; Sedbrook, D. F.; Krikorian, M.; Chen, J.; Sattler, A.; Carnes, M. E.; Murray, C. B.; Steigerwald, M.; Nuckolls, C., Functionalizing molecular wires: a tunable class of α,ω-diphenyl-μ,ν-dicyano-oligoenes. *Chem. Sci.* **2012,** *3*, 1007-1014.
58. Hong, W. J.; Manrique, D. Z.; Moreno-Garcia, P.; Gulcur, M.; Mishchenko, A.; Lambert, C. J.; Bryce, M. R.; Wandlowski, T., Single Molecular Conductance of Tolanes: Experimental and Theoretical Study on the Junction Evolution Dependent on the Anchoring Group. *J. Am. Chem. Soc.* **2012,** *134*, 2292-2304.
59. Maity, P.; Takano, S.; Yamazoe, S.; Wakabayashi, T.; Tsukuda, T., Binding Motif of Terminal Alkynes on Gold Clusters. *J. Am. Chem. Soc.* **2013,** *135*, 9450-9457.
60. Maity, P.; Xie, S. H.; Yamauchi, M.; Tsukuda, T., Stabilized gold clusters: from isolation toward controlled synthesis. *Nanoscale* **2012,** *4*, 4027-4037.
61. Maity, P.; Wakabayashi, T.; Ichikuni, N.; Tsunoyama, H.; Xie, S. H.; Yamauchi, M.; Tsukuda, T., Selective synthesis of organogold magic clusters $Au_{54}(C{\equiv}CPh)_{26}$. *Chem Commun* **2012,** *48*, 6085-6087.
62. Maity, P.; Tsunoyama, H.; Yamauchi, M.; Xie, S. H.; Tsukuda, T., Organogold Clusters Protected by Phenylacetylene. *J. Am. Chem. Soc.* **2011,** *133*, 20123-20125.
63. Herrer, L.; Gonzalez-Orive, A.; Marques-Gonzalez, S.; Martin, S.; Nichols, R. J.; Serrano, J. L.; Low, P. J.; Cea, P., Electrically transmissive alkyne-anchored monolayers on gold. *Nanoscale* **2019,** *11*, 7976-7985.
64. Osorio, H. M.; Cea, P.; Ballesteros, L. M.; Gascon, I.; Marques-Gonzalez, S.; Nichols, R. J.; Perez-Murano, F.; Low, P. J.; Martin, S., Preparation of nascent

molecular electronic devices from gold nanoparticles and terminal alkyne functionalised monolayer films. *J. Mater. Chem. C* **2014,** *2*, 7348-7355.
65. Olavarria-Contreras, I. J.; Perrin, M. L.; Chen, Z.; Klyatskaya, S.; Ruben, M.; van der Zant, H. S. J., C-Au Covalently Bonded Molecular Junctions Using Nonprotected Alkynyl Anchoring Groups. *J. Am. Chem. Soc.* **2016,** *138*, 8465-8469.
66. Bejarano, F.; Olavarria-Contreras, I. J.; Droghetti, A.; Rungger, I.; Rudnev, A.; Gutiérrez, D.; Mas-Torrent, M.; Veciana, J.; van der Zant, H. S. J.; Rovira, C.; Burzurí, E.; Crivillers, N., Robust Organic Radical Molecular Junctions Using Acetylene Terminated Groups for C–Au Bond Formation. *J. Am. Chem. Soc.* **2018,** *140*, 1691-1696.
67. Li, S.; Yu, H.; Chen, X.; Gewirth, A. A.; Moore, J. S.; Schroeder, C. M., Covalent Ag–C Bonding Contacts from Unprotected Terminal Acetylenes for Molecular Junctions. *Nano Lett.* **2020,** *20*, 5490-5495.
68. Zhao, X. T.; Huang, C. C.; Gulcur, M.; Batsanov, A. S.; Baghernejad, M.; Hong, W. J.; Bryce, M. R.; Wandlowski, T., Oligo(aryleneethynylene)s with Terminal Pyridyl Groups: Synthesis and Length Dependence of the Tunneling-to-Hopping Transition of Single-Molecule Conductances. *Chem. Mater.* **2013,** *25*, 4340-4347.
69. Lu, Q.; Liu, K.; Zhang, H. M.; Du, Z. B.; Wang, X. H.; Wang, F. S., From Tunneling to Hopping: A Comprehensive Investigation of Charge Transport Mechanism in Molecular Junctions Based on Oligo(p-phenylene ethynylene)s. *ACS Nano* **2009,** *3*, 3861-3868.
70. Low, P. J., Metal complexes in molecular electronics: progress and possibilities. *Dalton Trans* **2005**, 2821-2824.
71. Milan, D. C.; Vezzoli, A.; Planje, I. J.; Low, P. J., Metal bis(acetylide) complex molecular wires: concepts and design strategies. *Dalton Trans.* **2018,** *47*, 14125-14138.
72. Rigaut, S., Metal complexes in molecular junctions. *Dalton Trans.* **2013,** *42*, 15859-15863.
73. Higgins, S. J.; Nichols, R. J., Metal/molecule/metal junction studies of organometallic and coordination complexes; What can transition metals do for molecular electronics? *Polyhedron* **2018,** *140*, 25-34.
74. Evangeli, C.; Gillemot, K.; Leary, E.; Gonzalez, M. T.; Rubio-Bollinger, G.; Lambert, C. J.; Agrait, N., Engineering the Thermopower of C_{60} Molecular Junctions. *Nano Lett.* **2013,** *13*, 2141-2145.
75. Rincon-Garcia, L.; Evangeli, C.; Rubio-Bollinger, G.; Agrait, N., Thermopower measurements in molecular junctions. *Chem. Soc. Rev.* **2016,** *45*, 4285-4306.
76. Dekkiche, H.; Gemma, A.; Tabatabaei, F.; Batsanov, A. S.; Niehaus, T.; Gotsmann, B.; Bryce, M. R., Electronic conductance and thermopower of single-molecule junctions of oligo (phenyleneethynylene) derivatives. *Nanoscale* **2020,** *12*, 18908-18917.
77. Akkerman, H. B.; de Boer, B., Electrical conduction through single molecules and self-assembled monolayers. *J. Phys. Condens. Mat.* **2008,** *20*, 013001.
78. Markussen, T.; Settness, M.; Thygesen, K. S., Robust conductance of dumbbell molecular junctions with fullerene anchoring groups. *J. Chem. Phys.* **2011,** *135*, 144104.
79. Ferrer, J.; Lambert, C. J.; Garcia-Suarez, V. M.; Manrique, D. Z.; Visontai, D.; Oroszlany, L.; Rodriguez-Ferradas, R.; Grace, I.; Bailey, S. W. D.; Gillemot,

K.; Sadeghi, H.; Algharagholy, L. A., GOLLUM: a next-generation simulation tool for electron, thermal and spin transport. *New J. Phys.* **2014,** *16*, 093029.
80. Tanaka, Y.; Kiguchi, M.; Akita, M., Inorganic and Organometallic Molecular Wires for Single-Molecule Devices. *Chem. Eur. J.* **2017,** *23*, 4741-4749.
81. Gryn'ova, G.; Ollitrault, P. J.; Corminboeuf, C., Guidelines and diagnostics for charge carrier tuning in thiophene-based wires. *Phys. Chem. Chem. Phys.* **2017,** *19*, 23254-23259.
82. Brooke, C.; Vezzoli, A.; Higgins, S. J.; Zotti, L. A.; Palacios, J. J.; Nichols, R. J., Resonant transport and electrostatic effects in single-molecule electrical junctions. *Phys. Rev. B* **2015,** *91*, 1953438.
83. Yuan, L.; Franco, C.; Crivillers, N.; Mas-Torrent, M.; Cao, L.; Sangeeth, C. S. S.; Rovira, C.; Veciana, J.; Nijhuis, C. A., Chemical control over the energy-level alignment in a two-terminal junction. *Nat. Commun.* **2016,** *7*, 12066.
84. Stefani, D.; Weiland, K. J.; Skripnik, M.; Hsu, C. W.; Perrin, M. L.; Mayor, M.; Pauly, F.; van der Zant, H. S. J., Large Conductance Variations in a Mechanosensitive Single-Molecule Junction. *Nano Lett.* **2018,** *18*, 5981-5988.
85. Yzambart, G.; Rincon-Garcia, L.; Al-Jobory, A. A.; Ismael, A. K.; Rubio-Bollinger, G.; Lambert, C. J.; Agrait, N.; Bryce, M. R., Thermoelectric Properties of 2,7-Dipyridylfluorene Derivatives in Single-Molecule Junctions. *J. Phys. Chem. C* **2018,** *122*, 27198-27204.
86. Garner, M. H.; Li, H. X.; Chen, Y.; Su, T. A.; Shangguan, Z.; Paley, D. W.; Liu, T. F.; Ng, F.; Li, H. X.; Xiao, S. X.; Nuckolls, C.; Venkataraman, L.; Solomon, G. C., Comprehensive suppression of single-molecule conductance using destructive sigma-interference. *Nature* **2018,** *558*, 415-419.
87. Bu, D. L.; Xiong, Y. Q.; Tan, Y. N.; Meng, M.; Low, P. J.; Kuang, D. B.; Liu, C. Y., Understanding the charge transport properties of redox active metal-organic conjugated wires. *Chem Sci* **2018,** *9*, 3438-3450.
88. Luo, L. A.; Choi, S. H.; Frisbie, C. D., Probing Hopping Conduction in Conjugated Molecular Wires Connected to Metal Electrodes. *Chem. Mater.* **2011,** *23*, 631-645.
89. Poot, M.; Osorio, E.; O'Neill, K.; Thijssen, J. M.; Vanmaekelbergh, D.; van Walree, C. A.; Jenneskens, L. W.; van der Zant, H. S. J., Temperature dependence of three-terminal molecular junctions with sulfur end-functionalized tercyclohexylidenes. *Nano Lett.* **2006,** *6*, 1031-1035.
90. Sedghi, G.; Garcia-Suarez, V. M.; Esdaile, L. J.; Anderson, H. L.; Lambert, C. J.; Martin, S.; Bethell, D.; Higgins, S. J.; Elliott, M.; Bennett, N.; Macdonald, J. E.; Nichols, R. J., Long-range electron tunnelling in oligo-porphyrin molecular wires. *Nat. Nanotechnol* **2011,** *6*, 517-523.
91. Quinn, J. R.; Foss, F. W.; Venkataraman, L.; Breslow, R., Oxidation potentials correlate with conductivities of aromatic molecular wires. *J. Am. Chem. Soc.* **2007,** *129*, 12376-12377.
92. Zangmeister, C. D.; Picraux, L. B.; van Zee, R. D.; Yao, Y. X.; Tour, J. M., Energy-level alignment and work function shifts for thiol-bound monolayers of conjugated molecules self-assembled on Ag, Cu, Au, and Pt. *Chem. Phys. Lett.* **2007,** *442*, 390-393.
93. Kaliginedi, V.; Rudnev, A. V.; Moreno-Garcia, P.; Baghernejad, M.; Huang, C. C.; Hong, W. J.; Wandlowski, T., Promising anchoring groups for single-molecule conductance measurements. *Phys. Chem. Chem. Phys.* **2014,** *16*, 23529-23539.

94. Hihath, J.; Tao, N. J., The role of molecule-electrode contact in single-molecule electronics. *Semicond. Sci. Tech.* **2014,** *29*, 054007.
95. Jia, C. C.; Guo, X. F., Molecule-electrode interfaces in molecular electronic devices. *Chem. Soc. Rev.* **2013,** *42*, 5642-5660.
96. Zotti, L. A.; Kirchner, T.; Cuevas, J. C.; Pauly, F.; Huhn, T.; Scheer, E.; Erbe, A., Revealing the Role of Anchoring Groups in the Electrical Conduction Through Single-Molecule Junctions. *Small* **2010,** *6*, 1529-1535.
97. Sangtarash, S.; Huang, C. C.; Sadeghi, H.; Sorohhov, G.; Hauser, J.; Wandlowski, T.; Hong, W. J.; Decurtins, S.; Liu, S. X.; Lambert, C. J., Searching the Hearts of Graphene-like Molecules for Simplicity, Sensitivity, and Logic. *J. Am. Chem. Soc.* **2015,** *137*, 11425-11431.
98. Geng, Y.; Sangtarash, S.; Huang, C. C.; Sadeghi, H.; Fu, Y. C.; Hong, W. J.; Wandlowski, T.; Decurtins, S.; Lambert, C. J.; Liu, S. X., Magic Ratios for Connectivity-Driven Electrical Conductance of Graphene-like Molecules. *J. Am. Chem. Soc.* **2015,** *137*, 4469-4476.

For Table of Contents Use Only